Mixed ligand passivation as the origin of near-unity emission quantum yields in CsPbBr₃ nanocrystals

Yang Ding a,‡, Zhuoming Zhang a,‡, Stefano Toso a,b, Irina Gushchina a, Vadim Trepalin a, Kejia Shi a, Jeffrey W. Peng a,*, Masaru Kuno a,c,*

- ^a Department of Chemistry and Biochemistry, University of Notre Dame, Notre Dame, IN 46556 USA
- ^b Nanochemistry Department, Instituto Italiano di Tecnologia, Via Morego 30, 16163 Genova, Italy
- ^c Department of Physics, University of Notre Dame, Notre Dame, IN 46556 USA

*Email: <u>jpeng@nd.edu</u> *Email: <u>mkuno@nd.edu</u>

‡Y.D. and Z.Z. contributed equally to this paper.

ABSTRACT: Key features of syntheses, involving the quaternary ammonium passivation of CsPbBr3 nanocrystals (NCs), include stable, reproducible and large (often near-unity) emission quantum yields (QYs). The archetypical example involves didodecyl dimethyl ammonium (DDDMA+) passivated CsPbBr3 NCs where robust QYs stem from interactions between DDDMA+ and NC surfaces. Despite widespread adoption of this synthesis, specific ligand-NC surface interactions responsible for large DDDMA+-passivated NC QYs have not been fully established. Multidimensional nuclear magnetic resonance experiments now reveal a new DDDMA+-NC surface interaction, beyond established "tightly-bound" DDDMA+ interactions, which strongly affects observed emission QYs. Depending upon the existence of this new DDDMA+ coordination, NC QYs vary broadly between 60% and 85%. More importantly, these measurements reveal surface passivation through unexpected didodecyl ammonium (DDA+) that works in concert with DDDMA+, to produce near unity (i.e. >90%) QYs.

Introduction

Colloidal CsPbBr₃ nanocrystals (NCs) are the latest nanostructure paradigm for applications in photovoltaics¹, lighting^{2,3}, radiation detection⁴, and in semiconductor laser cooling.^{5,6} This is due, in large part, to sizable CsPbBr₃ NC emission quantum yields (QYs) that result from their intrinsic resistance to forming mid gap states.^{7,8} The absence of as made, unity QYs, however, points to the continued importance of effective NC surface passivation with suitable organic ligands.^{9–12}

The prototypical preparation for CsPbBr₃ NCs utilizes PbBr₂ as a Pb and Br precursor. Oleylamine (OLAm) and oleic acid (OA) are simultaneously added to passivate NC surfaces.⁹ De Roo *et al.* ¹³, however, have shown, using Nuclear Magnetic Resonance (NMR) spectroscopy, that oleylammonium -a primary ammonium species, resulting from OA protonation of OLAm- is the actual species passivating CsPbBr₃ NC surfaces. Unfortunately, its ready deprotonation leads to detachment, which adversely impacts the stability, reproducibility, and overall magnitude of NC QYs obtained using this approach.

In response to the issue, Manna and coworkers have proposed an alternative, two-step strategy to prepare high quality CsPbBr₃ NCs.^{11,14–16} First, OA-passivated NCs are synthesized using OA and didodecylamine (DDAm, which does not bind to NC surfaces) as surfactants. NCs are then resurfaced by exposing them to a solution of a quaternary

ammonium cations such as didodecyl dimethyl ammonium (DDDMA*) whose intrinsic resistance to deprotonation results in improved ligand stability constants. This leads to reproducible syntheses of near-unity QY NCs with excellent colloidal stability. Syntheses involving quaternary ammonium salts have therefore become the prevailing approach for producing high QY CsPbBr₃ NCs. 19-31

Despite mass adoption, the actual origin of quaternary ammonium ligand-NC surface interactions, responsible for large and stable emission QYs, remains unanswered. Although early NMR studies 11 have confirmed DDDMA passivation of NC surfaces, they have left unanswered the specific ligand-surface interactions, responsible for near-unity QYs.

Here, we probe the surface binding of DDDMA+ to CsP-bBr3 using a combination of NMR experiments, including Heteronuclear Single Quantum Correlation (HSQC) spectroscopy, Nuclear Overhauser Effect Spectroscopy (NOESY), and Diffusion Ordered Spectroscopy (DOSY). The results lead to a model for ligand-NC surface interactions that rationalizes the large and reproducible QYs of quaternary ammonium passivated CsPbBr3 NCs. We further discover an unexpected ligand passivation that involves surface didodecyl ammonium (DDA+), unique to near-unity QY ensembles. Its presence is posited to stem from the reaction of introduced amine and bromine precursors in quaternary ammonium-based syntheses.

Results and Discussion

DDDMA⁺-passivated CsPbBr₃ NCs were prepared following the original approach reported by Imran *et al.*¹¹ The synthesis utilizes Cs-Pb-oleate as metal precursors, benzoyl bromide (BzBr) as a bromine precursor, and OA, DDAm and DDDMA⁺ as surface passivating agents. Reactions are first conducted in the absence of DDDMA⁺ to generate NCs. DDDMA⁺ bromide salt is then introduced to finalize the surface passivation of produced NCs. More about the approach can be found in the SI and in Reference 11. All samples have been washed to remove excess ligands prior to analytical or optical measurements. Details of the specimen processing have been provided in the SI.

Figures 1a and **S1a,b** show transmission electron microscopy (TEM) images of resulting CsPbBr₃ NCs. For the particular ensemble shown, a mean edge length (*I*) is *l*=7.8±0.7 nm. **Figure S1c** shows an associated sizing histogram (*N*=100 NCs, ~8% size distribution). Absolute QY measurements, using an integrating sphere, reveal a corresponding ensemble QY of 84.2%. More notably, the synthesis yields reproducible QYs as highlighted by **Figure S2**, which summarizes absolute QYs measured across eight consecutive preparations. Evident is the uniformity of observed QYs, which yields an average value of 86.0±1.2%. Details of these absolute QY measurements have been provided in the Methods section. Resulting specimens are referred to as medium-QY NCs.

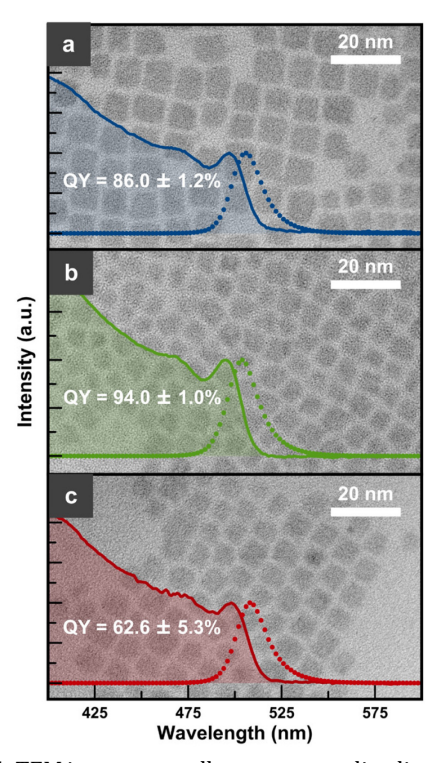


Figure 1. TEM images as well as corresponding linear absorption and photoluminescence spectra of representative (a) medium-, (b) high-, and (c) low-QY CsPbBr₃ NCs.

Subsequent X-ray diffraction (XRD) and selected area electron diffraction (SAED) patterns (**Figure S3**) match those expected for CsPbBr₃.³² Acquired linear absorption

and band edge emission spectra further agree with previously-established CsPbBr3 NC sizing curves33 and with reported, size-dependent Stokes shifts.34,35 TEM-based energy dispersive X-ray spectroscopy (TEM-EDXS) reveal that medium-QY NCs possess a lead- and bromine-rich stoichiometry of Cs:Pb:Br=1.0:1.3±0.2:3.8±0.2. This results from an introduced precursor (feed) stoichiometry of Cs:Pb:Br= 1.0:2.5:4.1 intended to yield a surface amenable to quaternary ammonium passivation. 11 For context, CsPbBr₃'s bulk stoichiometry is 1.0:1.0:3.0. The resulting NC surface is Br rich with ammonium ligands that replace nominal surface Cs+ cations. This surface passivation motif is referred to as ammonium-Br termination in what follows and is illustrated in the SI (Figure S4). Of note is that the measured NC stoichiometry agrees with the ideal ratios expected for *l*=6-8 nm ammonium-Br terminated CsP bBr_3 NCs (Cs:Pb:Br=1.0:1.2-1.3:4.0-4.5). 13,36,37 Details of TEM-EDXS measurements as well as ideal NC stoichiometry estimates have been provided in the Methods section and in the SI, respectively.

Given that the quality of ammonium-Br terminated NC surfaces is instrumental to achieving effective quaternary ammonium ligand passivation, observed QYs are likely sensitive to the relative excess of bromine introduced into preparations. In what follows, BzBr excesses introduced into preparations have therefore been varied while keeping feed Cs:Pb ratios constant at Cs:Pb=1.0:2.5.

These studies show that increasing the BzBr excess in the synthesis (feed stoichiometry: Cs:Pb:Br=1.0:2.5:8.4) increases the mean QY of eight sequential preparations to 94.0±1.0%. The measured TEM-EDXS stoichiometry (Cs:Pb:Br=1.0:1.3±0.1:4.1±0.2) again agrees with the *ideal* ratios expected for l=6-8 nm ammonium-Br terminated CsPbBr₃ NCs (Cs:Pb:Br=1.0:1.2-1.3:4.0-4.5). ^{13,36,37} **Figure S2** highlights the uniformity and reproducibility of these QYs.

In contrast, reducing the amount of BzBr added (feed stoichiometry: Cs:Pb:Br=1.0:2.5:2.1; subsequently measured TEM-EDXS stoichiometry: Cs:Pb:Br=1.0:1.0±0.1:3.5±0.2) lowers NC ensemble QYs to a mean value of 62.6±5.3% across eight sequential preparations (**Figure S2**). Low as made QYs suggest that produced NCs possess defective surfaces. This agrees with their less than ideal Cs:Pb:Br stoichiometries. The two produced, variable QY ensembles are referred to as high-and low-QY specimens. **Figures 1 b,c** and **S1d-i** summarize associated NC TEM images, sizing histograms, linear absorption, and band edge emission spectra.

Having established that variable Br excesses in preparations lead to statistically different NC QYs and that the near-ideal inorganic composition of medium- and high-QY NCs enable large QYs, we investigate their corresponding organic surface ligand passivation using NMR. Of particular interest is the surface passivation motif responsible for near-unity (i.e. >90%) QYs.

Figure 2 now shows ¹H-NMR spectra of high-, medium-, and low-QY CsPbBr₃ NCs suspended in toluene-d8. **Figures 2a-c** highlight three regions of interest (ROIs): 8.5-11.0 ppm (inset, **Figure 2a**), 2.3-4.7 ppm (**Figure 2b**),

and 0.7-2.1 ppm (**Figure 2c**). These ROIs are intended to better visualize DDDMA+ ammonium and alkylic chain protons. In parallel, NMR spectra of pure OA, DDAm, DDDMA+, and pure DDA+ have been acquired to better identify surface-bound species. DDA+ has been synthesized separately as described in the SI. Its ¹H spectrum has been recorded because it represents a potential byproduct, stemming from DDAm being protonated in the reaction medium. **Figure 2d** illustrates the chemical structures of DDDMA+ and DDA+ as well as the labeling of their ammonium and aliphatic protons. **Figure S5** summarizes ¹H peak assignments for above reference species. See also References 11 and 15.

Figure 2 reveals that high-, medium-, and low-QY samples all feature broad $^1\mathrm{H}$ resonances at ~ 4.0 , ~ 3.6 , ~ 1.4 , and ~ 1.3 ppm. Orange fills in **Figures 2b,c** highlight said resonances. These features are attributed to surface-bound DDDMA+ and match assignments previously made by Imran *et al.*¹¹ High-, medium-, and low-QY $^1\mathrm{H}$ NMR spectra further exclude non-protonated DDAm as a surface passivating agent due to absence of an α-methylene triplet at 2.56 ppm (**Figure S5e**). OA is also excluded because its ethylene linewidth and chemical shift at 5.46 ppm match those of free OA (**Figure S5f**).

Close inspection of **Figure 2** shows that distinguishing washed medium- and high-QY specimens from

corresponding low-QY ensembles are broad, blue-high-lighted $^1\mathrm{H}$ resonances in **Figures 2b,c**. These features resist multiple (i.e. two/three, **Figure S6**) washing steps and have *not* been observed in prior $^1\mathrm{H}$ NMR spectra of DDDMA+-passivated CsPbBr3 NCs. 11,23,24,30,31 Observed resonances are assigned to DDDMA+'s α -methyl, α -methylene, and alkylic chain protons. The assignments are supported by similar chemical shifts to orange-highlighted DDDMA+ resonances in **Figure 2**. They are further corroborated by the integrated 3:2 ratio of blue-highlighted peaks in **Figure 2b**, which match those of corresponding orange-highlighted peaks at $\sim\!4.0$ and $\sim\!3.6$ ppm for high-, medium-, and low-QY specimens. All follow the expected 3:2 ratio of integrated DDDMA+ α -methyl/ α -methylene resonances.

The data thus point to two surface-bound DDDMA+ moieties in high- and medium-QY specimens. Slight up-field/downfield shifts indicate that these newly observed, surface-bound DDDMA+ species reside in a different chemical environment, while different linewidths suggest different degrees of interaction with the NC surface. Newly-observed DDDMA+ α -methyl, α -methylene, and alkylic chain proton resonances are hereto forth denoted using asterisks (i.e. *DDDMA+ α -methylene, *DDDMA+ α -CH2- , *DDDMA+ α -CH2- , *DDDMA+ α -CH2- , and *DDDMA+ α -Me).

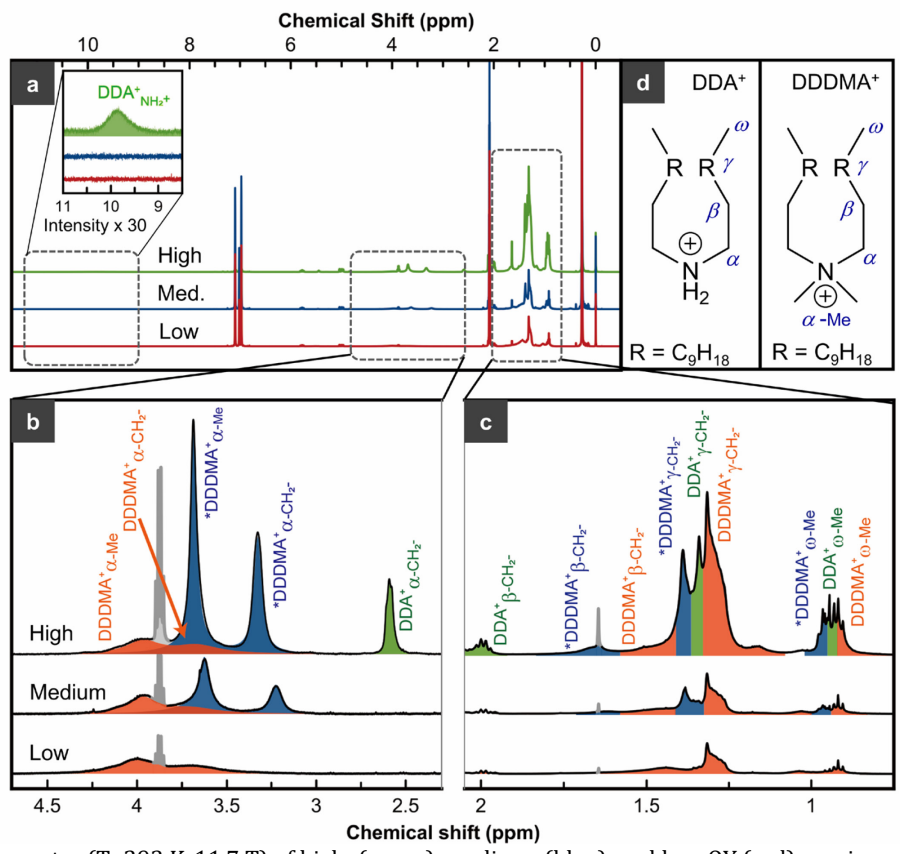


Figure 2. (a) ¹H-NMR spectra (T=293 K, 11.7 T) of high- (green), medium- (blue), and low-QY (red) specimens suspended in toluene-d8. Inset: enlarged ROI between 8.5-11.0 ppm. (b) ROI between 2.3-4.7 ppm. (c) ROI between 0.7-2.1 ppm. (d) Structures of DDA+ and DDDMA+ with important protons labeled.

Of added note is that **Figure 2** reveals high-QY specimens to possess unique ¹H resonances between 8.5-11.0 ppm and 0.7-2.6 ppm. These features are highlighted with green fills in **Figures 2a** (inset), **b**, and **c**. Such resonances have likewise not been reported previously and are not due to sample impurities, given their sizable abundance, even after extensive sample purification. See the SI and **Figure S6** for more details.

Systematic comparison of these unknown resonances with those of OA, DDAm, and DDDMA+ reveal no matches. The unknown resonances do, however, possess chemical shifts near identical to those of DDA+ (**Figure S5d**), a potential chemical byproduct of DDAm being protonated in the reaction medium. This is corroborated by crystalline DDABr (i.e. DDA+'s bromide salt) reflections seen in XRD patterns of high-QY specimens (**Figure S3**). Features at 9.88 ppm (inset, **Figure 2a**) and 2.58 ppm (**Figure 2b**) are therefore assigned to DDA+'s ammonium (DDA+ $_{\rm NH_2^+}$) and α -methylene (DDA+ $_{\alpha$ -CH2- $_{\rm CH2-}$) groups. Resonances at 2.00 ppm can likewise be linked to DDA+'s β -methylene (DDA+ $_{\beta$ -CH2- $_{\rm CH2-}$) groups (**Figure 2c**).

Additional features at 1.34 ppm and 0.94 ppm arise from DDA+'s alkylic chain (DDA+_CH2-) and terminal methyl (DDA+_M-Me) protons. These results point to DDA+ surface passivation as a distinct feature of high-QY NCs. It further suggests that DDA+ surface passivation is responsible, in whole or in part, to observed, near-unity QYs of quaternary ammonium-passivated NCs.

DDA+ and DDDMA+ assignments are confirmed using independent, two-dimensional (2D) ¹H-¹³C HSQC spectroscopies at natural abundance. In brief, HSQC measurements produce characteristic ¹H-¹³C cross peaks that link ¹H resonances of interest to established DDDMA+/*DDDMA+ (or DDA+) ¹³C resonances. From this, the lineage of posited ¹H resonances in **Figure 2** can be conclusively established.

To illustrate, ^{13}C resonances at 53 ppm and 64 ppm (**Figure S7**) correlate to previously assigned ^{1}H *DDDMA+ and *DDDMA+. resonances at ~3.6 ppm and ~3.2 ppm (blue fills, **Figure 2b**). The same ^{13}C resonances correlate to weak ^{1}H DDDMA+. and DDDMA+. features at ~4 ppm and ~3.6 ppm (orange fills, **Figure 2b**), in agreement with prior literature. The observed correlations thus establish the identity of The resonances between 3.0-4.5 ppm in **Figure 2b** to DDDMA+ and *DDDMA+. In the same way, DDA+'s The observed correlations thus establish the dentity of The resonance at 47 ppm (**Figure S7**) confirms assignment of **Figure 2b**'s 2.58 ppm feature to The DDA+. Additional details regarding these HSQC assignments can be found in the SI and in **Figure S7**.

To establish if and how above identified DDDMA⁺ and DDA⁺ moieties are surface-bound, NMR-based DOSY ³⁸ has been conducted on high-QY specimens that contain all resonances of interest. DOSY estimates ligand diffusion coefficients (*D*) with the implicit assumption that species possessing *D*-values smaller than those of corresponding free ligands are surface-bound.

DOSY results in **Figure S8** reveal DDDMA⁺ and *DDDMA⁺ D-values (D_{DDDMA^+} and $D_{\text{*}_{\text{DDDMA}^+}}$) smaller than

that of free DDDMA+. The DOSY results also show that $D_{
m DDDMA^+}$ and $D_{
m ^*DDDMA^+}$ differ: $D_{
m DDDMA^+} = 120 \pm 20~\mu m^2/s < D_{
m ^*DDDMA^+} = 295 \pm 52~\mu m^2/s < D_{
m free-DDDMA^+} = 540 \pm 87~\mu m^2/s.$ The same DOSY measurements reveal a DDA+ D-value smaller than that of free DDA+: D_{DDA} + =500±86 μ m²/s < $D_{\text{free-DDA}^+} = 670 \pm 90 \, \mu\text{m}^2/\text{s}$. Altogether, the results suggest that observed DDDMA+, *DDDMA+, and DDA+ are surface bound. However, different DDDMA+ and *DDDMA+ Dvalues imply that DDDMA+ experiences a stronger surfaceligand interaction than either *DDDMA+ or DDA+, as suggested by its broader ¹H-NMR resonances (see **Figure 2**). Similar observations have been reported for the surface passivation of ZnO, HfO₂, and CdSe NCs, where a mixed ligand shell, consisting of strongly and loosely bound moieties, is observed.^{39,40} The two identified surface-bound DDDMA⁺ species are consequently referred to as tightlyand loosely-bound DDDMA+.

¹H NMR and DOSY measurements suggest a structural model for the CsPbBr₃ NC surface, summarized in **Figure 3a**. Tightly-bound DDDMA⁺ occupies interstices between neighboring PbBr₆ octahedra (referred to as PbBr₆ interstices in what follows),¹¹.¹6,³⁰ Loosely-bound *DDDMA⁺ coordinate weakly to the NC surface, likely interacting with apical Br⁻ of terminal PbBr₆ octahedra via ammonium-Br hydrogen bonding and electrostatic interactions.²¹.⁴¹-⁴³ DDDMA⁺ and *DDDMA⁺ nominally exchange positions.

Molecular dynamics simulations indicate that the binding free energy of DDA+ to NC surface PbBr₆ interstices is more positive than that for DDDMA+.30 Predicted free energy differences are attributed to different DDDMA+/solvent versus DDA+/solvent interactions in the unbound state. Surface PbBr₆ interstices are therefore mainly occupied by (tightly-bound) DDDMA+.15,30 Consequently, surface-bound DDA+ likely coordinate to surface apical Br- much like *DDDMA+ (**Figure 3a**). Only high- and medium-QY NCs possess this dual passivation motif (interstice + apical) where *DDDMA+ and DDA+ prevent apical Br- from detaching from the NC surface. Low-QY specimens lack this stabilization due to their non-ideal surfaces.

The hypothesized high- and medium-QY NC surface model is then probed using 2D ¹H-¹H NOESY by identifying proton pairs in close proximity (≤0.5 nm).⁴⁴.⁴⁵ Interacting protons lead to cross peaks in NOESY spectra. **Figure 3b** shows the NOESY spectrum (16.4 T, 25 ms mixing time) of a high-QY NC ensemble between 1.0-4.5 ppm. Positive (negative) cross peaks are denoted black (red). **Figure S9** shows a full NOESY spectrum.

Figure 3b reveals multiple positive cross peaks (CPs), CPs 1-7, within three ROIs, distinguished by the chemical identity of interacting protons. ROI 1 (CPs 1-2) highlights interacting DDDMA⁺ and *DDDMA⁺ α -methyl and α -methylene protons. ROI 2 (CPs 3-5) highlights interacting DDA⁺ and DDDMA⁺/*DDDMA⁺ α -methyl and α -methylene protons. ROI 3 (CPs 6-7) shows interacting DDDMA⁺ and *DDDMA⁺ β -methylene protons.

Because NOESY cross peaks can also reflect chemical exchange, 2D ROESY (Rotating Frame Overhauser Effect Spectroscopy, 16.4 T, 20 ms mixing time) spectra have

simultaneously been recorded.⁴⁶ In ROESY, cross peaks indicating spatial proximity (black, negative) are of opposite sign compared to the diagonal. Cross peaks, arising from exchange (red, positive), adopt the same sign.

Figure 3c reveals a positive ROESY exchange cross peak (CP 1) between DDDMA+ and *DDDMA+. This indicates

their reversible binding to the NC surface. CP 2 exhibits a more complicated lineshape with a negative center and positive wings. The latter is attributed to DDDMA+/*DDDMA+ exchange while the former arises from the spatial proximity of *DDDMA+'s α -methyl and α -methylene protons.

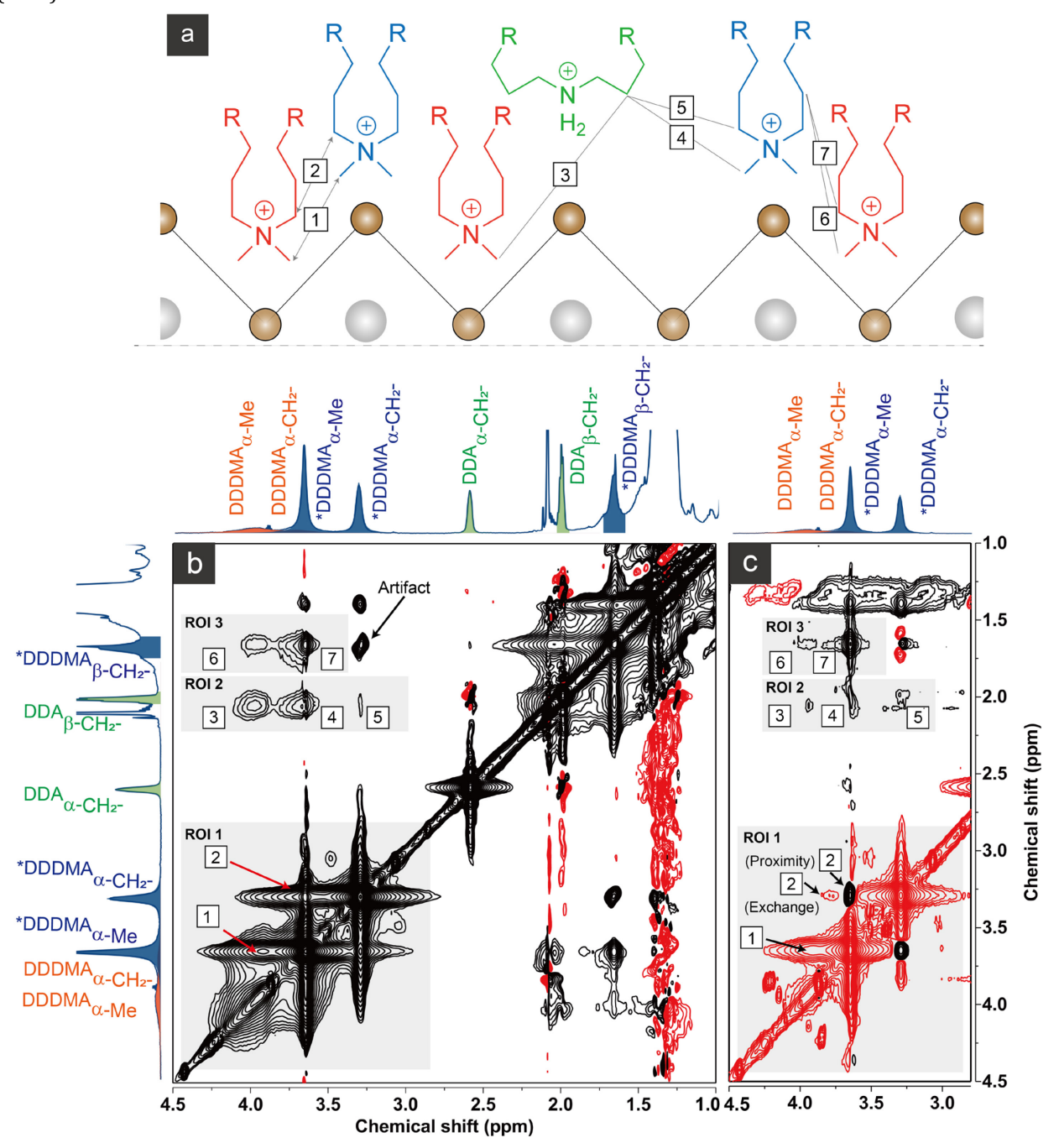


Figure 3. (a) Proposed surface model of high-QY NCs. Established NOESY interactions between DDDMA+ (red), *DDDMA+ (blue), and DDA+ (green) protons indicated using boxed numbers. (b) ¹H-¹H NOESY spectrum (25 ms mixing time) of high-QY NCs at 303 K, 16.4 T. Positive (negative) cross peaks indicated black (red). (c) Corresponding ROESY spectrum (10 ms CW spin lock, 7.14 kHz) acquired at 303 K and 16.4 T. Negative (positive) ROESY signals indicated black (red).

CPs 3-7 exhibit negative ROESY cross peaks. CPs 3-5 therefore point to spatial proximity of DDA+ and DDDMA+ as well as *DDDMA+ on the NC surface. CPs 6-7 indicate

spatial proximity of DDDMA⁺ and *DDDMA⁺. Because DDDMA⁺ has been established to be tightly bound to surface PbBr₆ interstices^{11,16,30}, the NOESY/ROSEY data in

Figure 3 support *DDDMA* and, by extension, DDA*, passivating apical Br. Due to the surface's complexity, however, full confirmation of the proposed microscopic surface passivation model awaits further studies. Additional details of these NOESY/ROESY analyses can be found in the SI along with **Figures S10** and **S11**, which provide both a full ROESY spectrum as well as additional NOESY spectra.

The developed surface model is corroborated by independent surface ligand density estimates in high-, medium-, and low-QY NCs. **Table 1** summarizes experimentally established surface ligand densities. For high-QY NCs, a nominal surface ligand density is 2.6 nm⁻². This is in near quantitative agreement with theoretical maximum ligand densities of 2.0-3.3 nm⁻² that account for organic ligand steric footprints between 0.3-0.5 nm^{2.47} Corresponding surface ligand densities for medium- and low-QY NCs are 1.5 nm⁻² and 1.0 nm⁻².

Near identical DDDMA⁺ densities between high-, medium-, and low-QY NCs in **Table 1**, suggest saturation of interstitial sites. Evident then is that major differences between NC types and their resulting emission QYs stem from *DDDMA⁺ passivation of apical Br⁻ sites in high- and medium-QY NCs and apical Br⁻ DDA⁺ passivation exclusive to high-QY specimens. Details of these surface density estimates have been provided in the SI along with **Figure S12**, which shows NMR and linear absorption spectra used to estimate values in **Table 1**.

Table 1. Surface ligand densities of high-, medium-, and low-QY NCs. Also included are corresponding values for medium-QY NCs made

using modified syntheses.

	Specimen	DDDMA+ (nm ⁻²)		DDA+ (apical)	Total (int. + ap.)
Specimen		DDDMA+ (interstitial)	*DDDMA+ (apical)	(nm ⁻²)	(nm ⁻²)
	Ideal	-	-	-	3.3
	High-QY	1.0	1.2	0.4	2.6
Med-QY Low-QY		1.0	0.5	-	1.5
		1.0	-	-	1.0
Mod. Med QY	DDA+ → DDDMA+	1.2	0.8	0.5	2.5
	DDDMA+ → DDA+	1.0	0.4	0.1	1.5

An important question that arises is the origin of unexpected DDA⁺ in high-QY specimens. ¹H-NMR spectra have therefore been acquired immediately after NCs have been synthesized but prior to their passivation with DDDMA⁺ (**Figures S13a,b**). Obtained spectra show that DDA⁺ is already present on NC surfaces. ¹⁵ This suggests that it originates from the reaction of precursors used in the synthesis. Although there exist many possible chemical routes to DDA⁺, likely pathways involve introduced BzBr reacting with DDAm and/or OA.

Figure S13c shows the ¹H NMR spectrum of a mixture of BzBr, DDAm, and OA. Concentrations have been chosen to mimic those used in actual CsPbBr₃ NC syntheses. The spectrum reveals near identical resonances (i.e. in terms of chemical shifts, multiplicities, and peak areas) to those observed from surface-bound DDA⁺ in high-QY NCs

(**Figure S13d**). The assignment is further confirmed by a characteristic ammonium singlet at 8.20 ppm. This control study confirms that excess BzBr in high-QY NC preparations reacts with other precursors introduced into the synthesis to produce in-situ DDA+ on NC surfaces.

To test whether deliberately added DDA+ improves medium- and high-QY NC surface passivation efficiencies and corresponding emission QYs, syntheses have been modified to allow DDA+ to be added to initially produced NCs prior to the introduction of DDDMA+ (denoted DDA+→DDDMA+). Details of modified syntheses have been provided in the SI. Results from these measurements are then compared to three control cases: (a) high- and medium-QY NCs prepared using standard syntheses (denoted standard). (b) high- and medium-OY NCs prepared using double the amount of DDDMA+ (denoted double DDDMA+), and (c) where additional DDA+ has been added to samples following their synthesis in (a) (denoted DDDMA+ \rightarrow DDA+). For all modifed corresponding ammonium bromide salts are used (i.e. DDDMABr and DDABr) with the total amount of Br present standardized at 102.83 nmol. Details of modified high- and medium-QY NC syntheses have been provided in the SI.

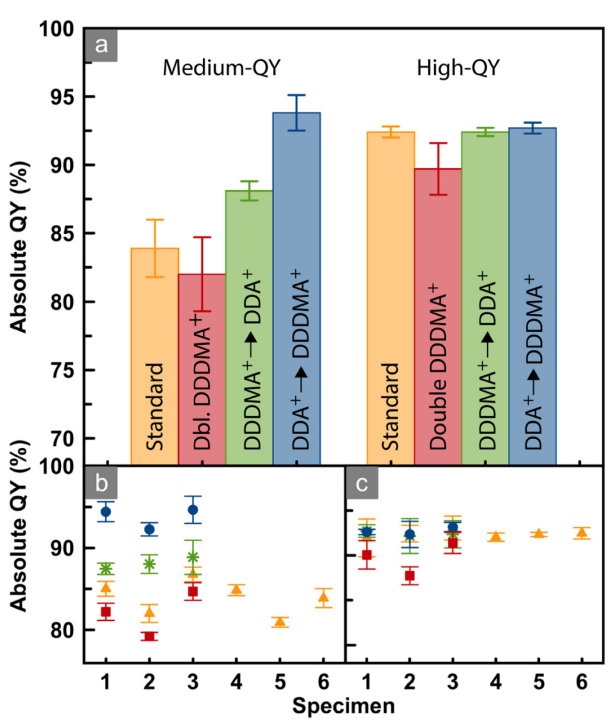


Figure 4. (a) Absolute QYs of modified medium- (left) and high-QY (right) NCs. From left to right: standard synthesis (yellow). Sample size = 6. Double DDDMA+ (red), DDDMA+ followed by DDA+ (green), and DDA+ followed by DDDMA+ (blue,). Sample size = 3 for double DDDMA+, DDDMA+→DDA+, and DDA+→DDDMA+. (b, c) Specific QYs of specimens used in (a). Error bars reflect QY measurements conducted in triplicate.

QYs of modified high- and medium-QY NCs (DDA+→DDDMA+, **Figure 4a**) are 92.7±0.4% and 93.8±1.3%, respectively. Those of specimens where DDA+ has been added following DDDMA+ addition

(DDDMA⁺→DDA⁺, **Figure 4a**) are 92.4±0.3% and 88.1±0.7%. These measurements show that deliberately adding DDA⁺ to medium-QY specimens increases their QYs. Those where double the amount of DDDMA⁺ has been added (double DDDMA⁺, **Figure 4a**) show QY drops to 89.7±1.9% and 82±2.7%. These measurements point to DDA⁺ being responsible for increasing medium-QY NC QYs. Adding DDA⁺ to high-QY specimens, however, results in little to no change of their QYs.

For medium-QY NCs, adding DDA⁺ increases their overall surface ligand densities (before: 1.5 nm⁻², after: 2.5 nm⁻²). This can be rationalized by DDA⁺'s smaller size compared to DDDMA⁺. What results are better passivated NCs with correspondingly larger emission QYs.

By contrast, adding DDA⁺ to NCs, following DDDMA⁺ passivation does not improve the surface passivation of medium-QY NCs (surface density before: 1.5 nm⁻², after ~1.5 nm⁻²). This likely stems from added DDA⁺ failing to effectively penetrate existing DDDMA⁺/*DDDMA⁺ mixed ligand shells on medium-QY NCs. Calculations for reported ligand densities are summarized in the SI along with employed quantitative ¹H NMR and linear absorption data (**Figure S14**). In high-QY NCs, negligible QY enhancement following DDA⁺ addition is attributed to their (existing) near ideal surface passivation (**Table 1**).

Of note is that only adding DDA+ yields tangible NC QY improvements. Both the above double DDDMA+ synthesis as well as post synthesis DDDMA+ titration measurements conducted on regular high- and medium-QY NCs yield negligible enhancements (**Figures S15** and **S16**). Regarding the latter DDDMA+ titration study, although initial DDDMA+ addition does increase emission quantum yields, we observe simultaneous etching of the NCs. This is evident through blueshifts of the NC absorption edge followed by the NCs becoming non-emissive in the limit of large DDDMA+ excess. These results thus point to DDA+ and similarly benign passivating agents as key to realizing near-unity QYs in quaternary ammonium passivated CsP-bBr₃ NCs.

Conclusion

Multidimensional NMR measurements of DDDMA+passivated CsPbBr₃ NCs reveal a dense shell of DDDMA+, *DDDMA+, and DDA+ passivating their surfaces. Tightlybound DDDMA+ moieties occupy terminal PbBr₆ interstices. They are augmented by loosely-bound *DDDMA+ and DDA+, which coordinate to apical Br- of terminal PbBr₆ octahedra. For high-QY NCs, what results is the near ideal passivation of both their interstitial and apical surface sites, aided by accidental DDA+ resulting from DDAm protonation in the reaction medium. Crucially, DDA+ is found to prefer apical Br⁻ sites more than DDDMA⁺, most likely by virtue of its lower steric encumbrance and the ability to form hydrogen bonds. This is, in turn, responsible for their near unity QYs. The resulting surface model and conclusions point to the importance of exploring mixed ligand surface passivation schemes for NCs, whether for shape control, colloidal stability, solubility in different solvents or for enhancing their emission QYs.

Methods

Optical Measurements. Absorption and photoluminescence spectroscopy. Linear absorption spectra were acquired using a Cary 50 Bio UV-vis spectrophotometer. Spectra were recorded under ambient conditions in 1 cm pathlength fused silica cuvettes using dilute solutions of NCs in toluene. Optical densities were kept below 0.3 in all cases

Photoluminescence QY measurements. PL QY measurements were conducted using an integrating sphere (Labsphere). A supercontinuum laser (NKT/Fianium, SC450), coupled to an acousto optical tunable filter, was used to excite specimens ($\lambda_{\rm exc}$ =450 nm). Excitation light was introduced into the integrating sphere using an optical fiber. Output light was collected using a second fiber and was sent to a fiber-based spectrometer (Ocean Insight, USB 2000+). The setup was calibrated using Rhodamine 110 (QY = 92%, 450 nm excitation) in ethanol (200 proof). ⁴⁸ All specimen optical densities were kept below 0.1 at 450 nm.

TEM and XRD measurements. TEM images were acquired using a JEOL 2011 microscope, operating an accelerating voltage of 200 kV. Samples were prepared by dropcasting dilute NC solutions in toluene onto ultrathin amorphous carbon substrates with copper supports (Ladd). Powder XRD measurements were acquired using a Bruker D8 Discover diffractometer with a Cu-K α source (λ =1.5418 Å). Measurements were conducted in the Bragg–Brentano geometry between 10-60° 20 with a step size of 0.01°. An integration time was four seconds per step.

NMR spectroscopy. One-dimensional ¹H-NMR spectra were acquired using a Bruker AVANCE III HD 500 MHz spectrometer (11.7 T). Spectral widths were 16 ppm with 128 transients accumulated in all experiments. Chemical shifts were calibrated using a tetramethylsilane (TMS) internal standard. NOESY spectra were collected on the AVANCE III spectrometer and a Bruker AVANCE I 700 MHz spectrometer (16.4 T). HSQC, DOSY, and ROESY measurements were exclusively conducted on the Bruker AVANCE I spectrometer.

 $^{1}H^{-13}C$ HSQC. Natural abundance 2D $^{1}H^{-13}C$ spectra were recorded at 16.4 T, 303 K. Each 2D dataset consisted of 256 FIDs (16 scans per FID), corresponding to 128 time increments in the ^{13}C dimension (t₁). Each FID consisted of 1024 complex data points for the ^{1}H dimension (t₂). The recycle delay was 1.5 seconds. Coherence-selection gradients provided sign-discrimination in t₁. The ^{1}H spectral width was 11.98 ppm, centered about 4.703 ppm; for ^{13}C it was 71 ppm, centered about 38 ppm.

DOSY spectroscopy. Samples consisted of 0.35 mM (0.83 mM) didodecyl dimethyl ammonium bromide, DDDMABr (didodecylammonium bromide, DDABr) in toluene-d8. The standard LED pulse scheme (Bruker pulse program "stebpsp1s")⁴⁹ and an in-house variant with a selective 1D TOCSY spin lock that preceded the stimulated echo was used to detect otherwise buried resonances. Stimulated echo parameters included a fixed diffusion time of Δ =60 ms and a δ =800 ms gradient pulse length.

DOSY data were collected as a pseudo 2D spectrum, consisting of 64 FIDs with 32 scans per FID and a 1.5 s recycle delay. Each FID corresponded to a different gradient amplitude taken from a linear ramp starting from 2% to 80% of the maximum (55 Gauss/cm). All measurements were conducted at 303 K.

 $^1H^{-1}H$ NOESY spectroscopy. 2D NOESY spectra were collected on a Bruker 500 MHz (11.4 T) AVANCE III system, and a 700 MHz (16.4 T) AVANCE I system equipped with a TCI cryoprobe. Data collected at 500 MHz consisted of 256 FIDs (128 t_1 increments); data collected at 700 MHz consisted of 384 FIDS (192 t_1 increments). In all cases, FIDs consisted of 2048 complex points in t_2 . The NOE mixing time at 500 MHz was 350 ms; at 700 MHz, mixing times included 10 ms, 25 ms, and 400 ms. At 700 MHz, spectral widths were 11.98 ppm, centered at 4.703 ppm.

 $^1H^{-1}H$ ROESY spectroscopy. 2D ROESY spectra were recorded at 16.4 T (700 MHz) with T=303 K and 313 K. The ROESY spin-lock consisted of 25 ms continuous wave irradiation applied at 4.703 ppm with rf field strength of 7.14 kHz. All other parameters matched those used for 2D NOESY measurements.

ASSOCIATED CONTENT

Supporting Information. This material is available free of charge via the Internet at http://pubs.acs.org.

Details of the CsPbBr3 NC synthesis and purification, representative TEM images of high-, medium-, and low-QY specimens, corresponding size histograms, QY reproducibility of high-, medium-, and low-QY NC specimens, XRD and SAED patterns of high-, medium-, low-QY specimens, ideal ammonium-Br terminated CsPbBr3 model, details of TEM-EDXS measurements and ideal stoichiometries for ammonium-Br terminated CsPbBr₃ NCs, ¹H NMR spectra and structural elucidation of ligand candidates in toluene-d8, details of high- and medium-QY specimen washing measurements, ¹H-¹³C HSQC spectra of free DDA+, free DDDMA+, and high-OY NCs in toluene-d8, DOSY spectra of free DDA+, free DDDMA+, and high-QY NCs in toluene-d8, full NOESY spectrum of high-QY NCs in toluene-d8, full ROESY spectrum of high-OY NCs in toluene-d8, details of 1D selective saturation NOESY experiments, temperature-dependent NOESY spectra of high-QY NCs, DDDMA+, and DDA+ in toluene-d8, details of NC surface ligand density estimates, quantitative ¹H NMR measurements and NC concentration estimates via absorption, details regarding the synthesis of DDABr. ¹H NMR spectra of high-OY NCs before/after DDDMA+ passivation. ¹H NMR spectra of pure DDABr and the reaction product of BzBr and DDAm/OA, both in DMSO-d6, details of modified NC syntheses involving DDA+ and corresponding ligand densities estimates, details of DDDMA+ titration measurements with corresponding photoluminescence spectra acquired during DDDMA+ titration.

AUTHOR INFORMATION

Corresponding Authors

Jeffery W. Peng --- Department of Chemistry and Biochemistry, Notre Dame 46556, Indiana, USA; Email: ipeng@nd.edu ORCID: 0000-0002-1226-3815

Masaru Kuno --- Department of Chemistry and Biochemistry, Notre Dame 46556, Indiana, USA; Email: mkuno@nd.edu ORCID: 0000-0003-4210-8514

Present Addresses

Yang Ding --- Department of Chemistry and Biochemistry, Notre Dame 46556, Indiana, USA; Email: yding8@nd.edu ORCID: 0000-0001-8437-3565

Zhuoming Zhang --- Department of Chemistry and Biochemistry, Notre Dame 46556, Indiana, USA; Email:

zzhang18@nd.edu

ORCID: 0000-0002-0507-3546

Stefano Toso --- Nanochemistry Department, Istituto Italiano di Tecnologia, Via Morego 30, 16163 Genova, Italy

ORCID: 0000-0002-1621-5888

Irina Gushchina --- Department of Chemistry and Biochemistry, Notre Dame 46556, Indiana, USA

ORCID: 0000-0001-6930-2101

Vadim Trepalin --- Department of Chemistry and Biochemistry, Notre Dame 46556, Indiana, USA ORCID: 0000-0003-0589-6515

Kejia Shi --- Department of Chemistry and Biochemistry, Notre Dame 46556, Indiana, USA ORCID: 0000-0001-7313-2205

Author contribution

Y. D. and Z. Z. contributed to the manuscript equally.

Notes

The authors declare no conflicts of interest.

ACKNOWLEDGMENT

Y.D. thanks Zhumin Zhang for helpful discussions on the synthesis of DDABr. Y.D. also thanks Dr. Evgenii Kovrigin for instruction on NMR spectroscopy. M.K. thanks the MURI:MARBLe project under the auspices of the Air Force Office of Scientific Research (award no. FA9550-16-1-0362) for financial support. M.K. and I.G. thank the Division of Materials Sciences and Engineering, Office of Basic Energy Sciences, U.S. Department of Energy (DOE) under Award DE-SC0014334 for partial financial support of this work. M.K. and V.T. thank the NSF (DMR-1952841) for partial financial support. The authors acknowledge the Magnetic Resonance Research Center at the University of Notre Dame for providing access to the Bruker AVANCE III HD 500.

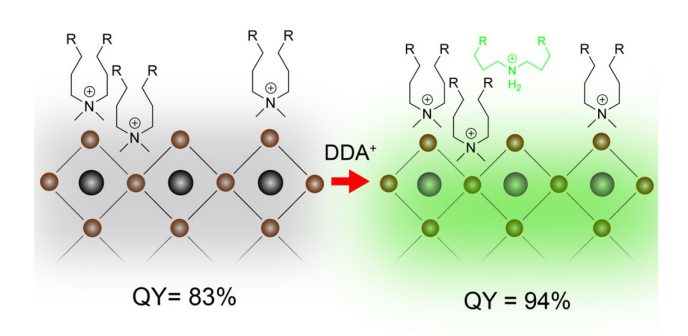
REFERENCES

- (1) Akkerman, Q. A.; Gandini, M.; Di Stasio, F.; Rastogi, P.; Palazon, F.; Bertoni, G.; Ball, J. M.; Prato, M.; Petrozza, A.; Manna, L. Strongly Emissive Perovskite Nanocrystal Inks for High-Voltage Solar Cells. *Nat. Energy* 2016, 2 (2), 16194. DOI: 10.1038/nenergy.2016.194.
- (2) Li, G.; Huang, J.; Zhu, H.; Li, Y.; Tang, J.-X.; Jiang, Y. Surface Ligand Engineering for Near-Unity Quantum Yield Inorganic Halide Perovskite QDs and High-Performance QLEDs. Chem. Mater. 2018, 30 (17), 6099–6107. DOI: 10.1021/acs.chemmater.8b02544.
- (3) Du, X.; Wu, G.; Cheng, J.; Dang, H.; Ma, K.; Zhang, Y.-W.; Tan, P.-F.; Chen, S. High-Quality CsPbBr₃ Perovskite Nanocrystals for Quantum Dot Light-Emitting Diodes. RSC Adv. 2017, 7 (17), 10391–10396. DOI: 10.1039/C6RA27665B.
- (4) Zhang, H.; Yang, Z.; Zhou, M.; Zhao, L.; Jiang, T.; Yang, H.; Yu, X.; Qiu, J.; Yang, Y. (Michael); Xu, X. Reproducible X-Ray

- Imaging with a Perovskite Nanocrystal Scintillator Embedded in a Transparent Amorphous Network Structure. *Adv. Mater.* **2021**, *33* (40), 2102529. DOI: 10.1002/adma.202102529.
- (5) Zhang, S.; Zhukovskyi, M.; Jankó, B.; Kuno, M. Progress in Laser Cooling Semiconductor Nanocrystals and Nanostructures. NPG Asia Mater. 2019, 11 (1), 54. DOI: 10.1038/s41427-019-0156-4.
- (6) Morozov, Y. V.; Zhang, S.; Brennan, M. C.; Janko, B.; Kuno, M. Photoluminescence Up-Conversion in CsPbBr₃ Nanocrystals. ACS Energy Lett. 2017, 2 (10), 2514–2515. DOI: 10.1021/acsenergylett.7b00902.
- (7) Huang, H.; Bodnarchuk, M. I.; Kershaw, S. V.; Kovalenko, M. V.; Rogach, A. L. Lead Halide Perovskite Nanocrystals in the Research Spotlight: Stability and Defect Tolerance. ACS Energy Lett. 2017, 2 (9), 2071–2083. DOI: 10.1021/acsenergylett.7b00547.
- (8) Kang, J.; Wang, L.-W. High Defect Tolerance in Lead Halide Perovskite CsPbBr₃. J. Phys. Chem. Lett. 2017, 8 (2), 489– 493. DOI: 10.1021/acs.jpclett.6b02800.
- (9) Protesescu, L.; Yakunin, S.; Bodnarchuk, M. I.; Krieg, F.; Caputo, R.; Hendon, C. H.; Yang, R. X.; Walsh, A.; Kovalenko, M. V. Nanocrystals of Cesium Lead Halide Perovskites (CsPbX₃, X = Cl, Br, and I): Novel Optoelectronic Materials Showing Bright Emission with Wide Color Gamut. *Nano Lett.* **2015**, *15* (6), 3692–3696. DOI: 10.1021/nl5048779.
- (10) Koscher, B. A.; Swabeck, J. K.; Bronstein, N. D.; Alivisatos, A. P. Essentially Trap-Free CsPbBr₃ Colloidal Nanocrystals by Postsynthetic Thiocyanate Surface Treatment. *J. Am. Chem. Soc.* 2017, 139 (19), 6566–6569. DOI: 10.1021/jacs.7b02817.
- (11) Imran, M.; Ijaz, P.; Goldoni, L.; Maggioni, D.; Petralanda, U.; Prato, M.; Almeida, G.; Infante, I.; Manna, L. Simultaneous Cationic and Anionic Ligand Exchange For Colloidally Stable CsPbBr₃ Nanocrystals. ACS Energy Lett. 2019, 4 (4), 819– 824. DOI: 10.1021/acsenergylett.9b00140.
- (12) Ravi, V. K.; Santra, P. K.; Joshi, N.; Chugh, J.; Singh, S. K.; Rensmo, H.; Ghosh, P.; Nag, A. Origin of the Substitution Mechanism for the Binding of Organic Ligands on the Surface of CsPbBr₃ Perovskite Nanocubes. *J. Phys. Chem. Lett.* 2017, 8 (20), 4988–4994. DOI: 10.1021/acs.jpclett.7b02192.
- (13) De Roo, J.; Ibáñez, M.; Geiregat, P.; Nedelcu, G.; Walravens, W.; Maes, J.; Martins, J. C.; Van Driessche, I.; Kovalenko, M. V.; Hens, Z. Highly Dynamic Ligand Binding and Light Absorption Coefficient of Cesium Lead Bromide Perovskite Nanocrystals. ACS Nano 2016, 10 (2), 2071–2081. DOI: 10.1021/acsnano.5b06295.
- (14) Imran, M.; Caligiuri, V.; Wang, M.; Goldoni, L.; Prato, M.; Krahne, R.; De Trizio, L.; Manna, L. Benzoyl Halides as Alternative Precursors for the Colloidal Synthesis of Lead-Based Halide Perovskite Nanocrystals. J. Am. Chem. Soc. 2018, 140 (7), 2656–2664. DOI: 10.1021/jacs.7b13477.
- (15) Imran, M.; Ijaz, P.; Baranov, D.; Goldoni, L.; Petralanda, U.; Akkerman, Q.; Abdelhady, A. L.; Prato, M.; Bianchini, P.; Infante, I.; Manna, L. Shape-Pure, Nearly Monodispersed CsP-bBr₃ Nanocubes Prepared Using Secondary Aliphatic Amines. *Nano Lett.* 2018, 18 (12), 7822–7831. DOI: 10.1021/acs.nanolett.8b03598.
- (16) Bodnarchuk, M. I.; Boehme, S. C.; ten Brinck, S.; Bernasconi, C.; Shynkarenko, Y.; Krieg, F.; Widmer, R.; Aeschlimann, B.; Günther, D.; Kovalenko, M. V.; Infante, I. Rationalizing and Controlling the Surface Structure and Electronic Passivation of Cesium Lead Halide Nanocrystals. ACS Energy Lett. 2019, 4 (1), 63–74. DOI: 10.1021/acsenergylett.8b01669.
- (17) Higginson, K. A.; Kuno, M.; Bonevich, J.; Qadri, S. B.; Yousuf, M.; Mattoussi, H. Synthesis and Characterization of Colloidal

- β-HgS Quantum Dots. J. Phys. Chem. B **2002**, 106 (39), 9982–9985. DOI: 10.1021/jp026232x.
- (18) Kuno, M.; Higginson, K. A.; Qadri, S. B.; Yousuf, M.; Lee, S. H.; Davis, B. L.; Mattoussi, H. Molecular Clusters of Binary and Ternary Mercury Chalcogenides: Colloidal Synthesis, Characterization, and Optical Spectra. J. Phys. Chem. B 2003, 107 (24), 5758–5767. DOI: 10.1021/jp0274684.
- (19) Palei, M.; Imran, M.; Biffi, G.; Manna, L.; Di Stasio, F.; Krahne, R. Robustness to High Temperatures of Al₂O₃-Coated CsP-bBr₃ Nanocrystal Thin Films with High-Photoluminescence Quantum Yield for Light Emission. ACS Appl. Nano Mater. 2020, 3 (8), 8167–8175. DOI: 10.1021/acsanm.0c01525.
- (20) Li, Z.; Kong, L.; Huang, S.; Li, L. Highly Luminescent and Ultrastable CsPbBr₃ Perovskite Quantum Dots Incorporated into a Silica/Alumina Monolith. *Angew. Chem. Int. Ed.* 2017, 56 (28), 8134–8138. DOI: 10.1002/anie.201703264.
- (21) Li, X.; Cai, W.; Guan, H.; Zhao, S.; Cao, S.; Chen, C.; Liu, M.; Zang, Z. Highly Stable CsPbBr₃ Quantum Dots by Silica-Coating and Ligand Modification for White Light-Emitting Diodes and Visible Light Communication. *Chem. Eng. J.* 2021, 419, 129551. DOI: 10.1016/j.cej.2021.129551.
- (22) Zheng, C.; Bi, C.; Huang, F.; Binks, D.; Tian, J. Stable and Strong Emission CsPbBr₃ Quantum Dots by Surface Engineering for High-Performance Optoelectronic Films. ACS Appl. Mater. Interfaces 2019, 11 (28), 25410–25416. DOI: 10.1021/acsami.9b07818.
- [23] Imran, M.; Ramade, J.; Di Stasio, F.; De Franco, M.; Buha, J.; Van Aert, S.; Goldoni, L.; Lauciello, S.; Prato, M.; Infante, I.; Bals, S.; Manna, L. Alloy CsCd_xPb_{1-x}Br₃ Perovskite Nanocrystals: The Role of Surface Passivation in Preserving Composition and Blue Emission. *Chem. Mater.* **2020**, *32* (24), 10641–10652. DOI: 10.1021/acs.chemmater.0c03825.
- (24) Abiodun, S. L.; Pellechia, P. J.; Greytak, A. B. Effective Purification of CsPbBr₃ Nanocrystals with High Quantum Yield and High Colloidal Stability via Gel Permeation Chromatography. *J. Phys. Chem. C* **2021**, *125* (6), 3463–3471. DOI: 10.1021/acs.jpcc.1c00207.
- (25) Baranov, D.; Fieramosca, A.; Yang, R. X.; Polimeno, L.; Lerario, G.; Toso, S.; Giansante, C.; Giorgi, M. D.; Tan, L. Z.; Sanvitto, D.; Manna, L. Aging of Self-Assembled Lead Halide Perovskite Nanocrystal Superlattices: Effects on Photoluminescence and Energy Transfer. ACS Nano 2021, 15. DOI: 10.1021/acsnano.0c06595.
- [26] Zhang, Z.; Zhang, S.; Gushchina, I.; Guo, T.; Brennan, M. C.; Pavlovetc, I. M.; Grusenmeyer, T. A.; Kuno, M. Excitation Energy Dependence of Semiconductor Nanocrystal Emission Quantum Yields. J. Phys. Chem. Lett. 2021, 12 (16), 4024–4031. DOI: 10.1021/acs.jpclett.1c00811.
- (27) DuBose, J. T.; Kamat, P. V. Surface Chemistry Matters. How Ligands Influence Excited State Interactions between CsPbBr₃ and Methyl Viologen. J. Phys. Chem. C 2020, 124 (24), 12990–12998. DOI: 10.1021/acs.jpcc.0c03004.
- (28) Balakrishnan, S. K.; Kamat, P. V. Ligand Assisted Transformation of Cubic CsPbBr₃ Nanocrystals into Two-Dimensional CsPb₂Br₅ Nanosheets. *Chem. Mater.* **2018**, *30* (1), 74–78. DOI: 10.1021/acs.chemmater.7b04142.
- (29) Gutiérrez Álvarez, S.; Lin, W.; Abdellah, M.; Meng, J.; Žídek, K.; Pullerits, T.; Zheng, K. Charge Carrier Diffusion Dynamics in Multisized Quaternary Alkylammonium-Capped CsPbBr₃ Perovskite Nanocrystal Solids. ACS Appl. Mater. Interfaces 2021, 13 (37), 44742–44750. DOI: 10.1021/acsami.1c11676.
- (30) Stelmakh, A.; Aebli, M.; Baumketner, A.; Kovalenko, M. V. On the Mechanism of Alkylammonium Ligands Binding to the Surface of CsPbBr₃ Nanocrystals. *Chem. Mater.* **2021**, *33* (15), 5962–5973. DOI: 10.1021/acs.chemmater.1c01081.

- (31) Abiodun, S. L.; Gee, M. Y.; Greytak, A. B. Combined NMR and Isothermal Titration Calorimetry Investigation Resolves Conditions for Ligand Exchange and Phase Transformation in CsPbBr₃ Nanocrystals. *J. Phys. Chem. C* **2021**, *125* (32), 17897–17905. DOI: 10.1021/acs.jpcc.1c00144.
- (32) Brennan, M. C.; Kuno, M.; Rouvimov, S. Crystal Structure of Individual CsPbBr₃ Perovskite Nanocubes. *Inorg. Chem.* 2019, 58 (2), 1555–1560. DOI: 10.1021/acs.inorgchem.8b03078.
- (33) Kuno, M.; Gushchina, I.; Toso, S.; Trepalin, V. No One Size Fits All: Semiconductor Nanocrystal Sizing Curves. J. Phys. Chem. C 2022, 126 (29), 11867–11874. DOI: 10.1021/acs.jpcc.2c04734.
- (34) Brennan, M. C.; Herr, J. E.; Nguyen-Beck, T. S.; Zinna, J.; Draguta, S.; Rouvimov, S.; Parkhill, J.; Kuno, M. Origin of the Size-Dependent Stokes Shift in CsPbBr₃ Perovskite Nanocrystals. J. Am. Chem. Soc. 2017, 139 (35), 12201–12208. DOI: 10.1021/jacs.7b05683.
- (35) Brennan, M. C.; Forde, A.; Zhukovskyi, M.; Baublis, A. J.; Morozov, Y. V.; Zhang, S.; Zhang, Z.; Kilin, D. S.; Kuno, M. Universal Size-Dependent Stokes Shifts in Lead Halide Perovskite Nanocrystals. J. Phys. Chem. Lett. 2020, 11 (13), 4937–4944. DOI: 10.1021/acs.jpclett.0c01407.
- (36) Maes, J.; Balcaen, L.; Drijvers, E.; Zhao, Q.; De Roo, J.; Vantomme, A.; Vanhaecke, F.; Geiregat, P.; Hens, Z. Light Absorption Coefficient of CsPbBr₃ Perovskite Nanocrystals. *J. Phys. Chem. Lett.* 2018, 9 (11), 3093–3097. DOI: 10.1021/acs.jpclett.8b01065.
- (37) Chen, Y.; Smock, S. R.; Flintgruber, A. H.; Perras, F. A.; Brutchey, R. L.; Rossini, A. J. Surface Termination of CsPbBr₃ Perovskite Quantum Dots Determined by Solid-State NMR Spectroscopy. J. Am. Chem. Soc. 2020, 142 (13), 6117–6127. DOI: 10.1021/jacs.9b13396.
- (38) Morris, K. F.; Johnson, C. S. Jr. Resolution of Discrete and Continuous Molecular Size Distributions by Means of Diffusion-Ordered 2D NMR Spectroscopy. J. Am. Chem. Soc. 1993, 115 (10), 4291–4299. DOI: 10.1021/ja00063a053.
- (39) Valdez, C. N.; Schimpf, A. M.; Gamelin, D. R.; Mayer, J. M. Low Capping Group Surface Density on Zinc Oxide Nanocrystals. ACS Nano 2014, 8 (9), 9463–9470. DOI: 10.1021/nn503603e.
- (40) De Roo, J.; Justo, Y.; De Keukeleere, K.; Van den Broeck, F.; Martins, J. C.; Van Driessche, I.; Hens, Z. Carboxylic-Acid-



TOC Figure

- Passivated Metal Oxide Nanocrystals: Ligand Exchange Characteristics of a New Binding Motif. *Angew. Chem. Int. Ed.* **2015**, *54* (22), 6488–6491. DOI: 10.1002/anie.201500965.
- (41) Kazes, M.; Udayabhaskararao, T.; Dey, S.; Oron, D. Effect of Surface Ligands in Perovskite Nanocrystals: Extending in and Reaching Out. Acc. Chem. Res. 2021, 54 (6), 1409–1418. DOI: 10.1021/acs.accounts.0c00712.
- (42) Vighnesh, K.; Wang, S.; Liu, H.; Rogach, A. L. Hot-Injection Synthesis Protocol for Green-Emitting Cesium Lead Bromide Perovskite Nanocrystals. ACS Nano 2022, 16 (12), 19618–19625. DOI: 10.1021/acsnano.2c11689.
- (43) Pan, A.; He, B.; Fan, X.; Liu, Z.; Urban, J. J.; Alivisatos, A. P.; He, L.; Liu, Y. Insight into the Ligand-Mediated Synthesis of Colloidal CsPbBr₃ Perovskite Nanocrystals: The Role of Organic Acid, Base, and Cesium Precursors. ACS Nano 2016, 10 (8), 7943–7954. DOI: 10.1021/acsnano.6b03863.
- (44) Hens, Z.; Martins, J. C. A Solution NMR Toolbox for Characterizing the Surface Chemistry of Colloidal Nanocrystals. Chem. Mater. 2013, 25 (8), 1211–1221. DOI: 10.1021/cm303361s.
- (45) Jeener, J.; Meier, B. H.; Bachmann, P.; Ernst, R. R. Investigation of Exchange Processes by Two-dimensional NMR Spectroscopy. J. Chem. Phys. 1979, 71 (11), 4546–4553. DOI: 10.1063/1.438208.
- (46) Bothner-By, A. A.; Stephens, R. L.; Lee, J.; Warren, C. D.; Jeanloz, R. W. Structure Determination of a Tetrasaccharide: Transient Nuclear Overhauser Effects in the Rotating Frame. J. Am. Chem. Soc. 1984, 106 (3), 811–813. DOI: 10.1021/ja00315a069.
- (47) Smock, S. R.; Chen, Y.; Rossini, A. J.; Brutchey, R. L. The Surface Chemistry and Structure of Colloidal Lead Halide Perovskite Nanocrystals. *Acc. Chem. Res.* 2021, 54 (3), 707–718. DOI: 10.1021/acs.accounts.0c00741.
- (48) Kubin, R. F.; Fletcher, A. N. Fluorescence Quantum Yields of Some Rhodamine Dyes. J. Lumin. 1982, 27 (4), 455–462. DOI: 10.1016/0022-2313(82)90045-X.
- (49) Gibbs, S. J.; Johnson, C. S. A PFG NMR Experiment for Accurate Diffusion and Flow Studies in the Presence of Eddy Currents. *J. Magn. Reson.* 1969 **1991**, 93 (2), 395–402. DOI: 10.1016/0022-2364(91)90014-K.